Turning Maneuvers of an Octopus-inspired Multi-arm Robotic Swimmer

Michael Sfakiotakis, Asimina Kazakidi and Dimitris P. Tsakiris

***Abstract*— Inspired by the agile underwater maneuvering of the octopus, an eight-arm robotic swimmer was developed. Associated dynamical models are used here to design turning maneuvers, an important ability for underwater navigation. The performance of several turning gaits, based on sculling arm movements, of this robotic system was investigated in simulation, with respect to their various kinematic parameters. Experiments with a prototype robotic swimmer confirmed the computational results and verified the multi-arm maneuverability of such systems.**

***Index Terms*— Biologically-Inspired Robots, Underwater Propulsion, Gaits, Octopus.**

I. INTRODUCTION

The dynamics of turning in aquatic animals has received little in-depth attention, as compared to straight-line locomotion, despite being the most prevalent behavior in nature. Marine animals spend a considerable amount of time, during their course of locomotion, in varying the speed, the acceleration and the heading direction, in order to follow a particular track. Turning is commonly achieved by the generation of asymmetrical lateral forces; for example, in fish, by differentiating the motion of their pectoral fins [1]. In the octopus, a cephalopod lacking fins, turning behaviors have not been investigated in detail. However, biological observations of arm swimming suggest that turning mechanisms may involve asymmetric movements of the arms; in the more predominant swimming mechanism of jetting, the redirection of the siphon and the non-uniform filling of the mantle may be used for steering [2].

Based on the octopus anatomy, we developed a dynamical model of an 8-arm robotic swimmer and a robotic prototype device, for underwater experimentation [3]. The model includes accurate fluid drag information, obtained by computational fluid dynamics (CFD) methods [4], namely the normalized normal and tangential fluid drag coefficients for various arm-like configurations [5]. Both the model and the robotic swimmer were tested for the generation of forward motion under sculling movements (for definition, see Section III) and arm undulations, or combinations of both, revealing substantial forward propulsion capabilities for the system.

This work was supported in part by the European Commission via the ICT-FET OCTOPUS Integrated Project, under contract No. 231608, and by the ESF-GSRT HYDRO-ROB Project [PE7(281)].

M. Sfakiotakis, A. Kazakidi and D.P. Tsakiris are with the Institute of Computer Science, Foundation for Research and Technology – Hellas (FORTH), N. Plastira 100, Vassilika Vouton, GR-70013, Heraklion, Greece. M. Sfakiotakis is also with the Dept. of Electrical Engineering, Technological Educational Institute of Crete, Heraklion, Greece. {sfakios, kazakidi, tsakiris}@ics.forth.gr.

Our aim is to investigate whether such capabilities could be exploited in underwater robotic devices, so that they may use the same compliant robotic arms for both manipulation and propulsion. The use of such multi-function manipulators, inspired by the octopus arms [6]–[9], will greatly enhance the efficiency of underwater robotic applications. In line with this aim, in this paper, we focus on the maneuvering performance of the 8-arm swimmer of [3]. Both simulations and experiments were performed under various turning gaits. The effect of various kinematic parameters on the efficiency of the turning maneuvers was investigated.

Section II presents the computational framework of the 8-arm dynamical model used for the simulations. A kinematic parameter analysis on the maneuvering performance of this model is described in Section III. Section IV presents experimental results with the 8-arm robotic swimmer and Section V gives the final conclusions and discusses future directions of this work.

II. COMPUTATIONAL MODEL

Inspired by the anatomy of the octopus arms and body, which is known to exhibit bilateral symmetry (Fig. 1), the current study uses an 8-arm mechanical model, as shown in Fig. 2 [3], to investigate turning. The model considers a body in the shape of a disk (of diameter D), at the circumference of which, eight octopus-like arms are attached axisymmetrically, at intervals of $45°$. The arms are composed of kinematic chains of $n = 10$ cylindrical segments, interlinked by planar rotary joints of 1 dof, and are oriented such that diametrically-opposite pairs of arms move in the same plane. To allow correlation with the standard anatomical notation used for the octopus arms (Fig. 1), each arm of the computational model is assigned a similar notation, thus distinguishing the arms into four left (L) and four right (R) arms (as shown in Fig. 2a).

The 8-arm mechanical model is assumed to move within quiescent fluid, so that hydrodynamic forces acting on a single arm segment result only from its motion. Further, the model is considered to move at speeds at which the generated fluid forces are inertial and prevail over viscous fluid forces ($400 < Re < 4 \cdot 10^5$, where Re is the Reynolds number, a non-dimensional parameter characterizing the flow). Lastly, it is assumed that all three components of the total flow-induced force (tangential, F_T, normal, F_N, and lateral, F_L, fluid forces) are decoupled. These three approximations form the basis of the fluid drag model used here for simulating the interaction of each individual segment of the mechanical model with the surrounding fluid. Accordingly, the fluid

Preprint submitted to 21st Mediterranean Conference on Control and Automation.
Received February 22, 2013.

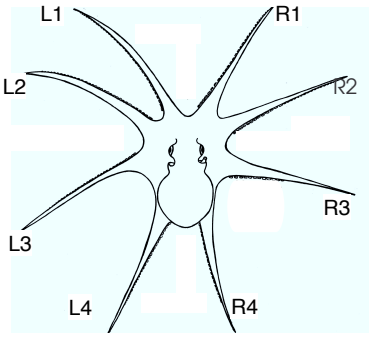

Fig. 1: Standard anatomical arm notation for the octopus (L: Left, R: Right). [10]

forces can be expressed as follows:

$$F_{i,\mathrm{dir}} = -\lambda_{i,\mathrm{dir}}\,\mathrm{sgn}(v_{i,\mathrm{dir}})\cdot(v_{i,\mathrm{dir}})^2,\ \mathrm{dir}=\{T,N,L\} \quad (1)$$

where $v_{i,T}$, $v_{i,N}$ and $v_{i,L}$ are the tangential, normal and lateral velocity components, respectively, of the ith segment, and $\lambda_{i,T}$, $\lambda_{i,N}$ and $\lambda_{i,L}$ are the fluid drag coefficients on the ith segment, corresponding to each fluid force component. However, the normal and lateral components are equal (i.e., $\lambda_{i,N}$=$\lambda_{i,L}$), as a result of the axial symmetry of the arm segments. Such resistive fluid drag models originate from studies of swimming animals [11] and are common in the robotic literature of bio-inspired elongated underwater systems (e.g., [12]–[14]). This approach is further validated by computational fluid dynamics (CFD) studies, as described in [5] and [4], the results of which were used for the estimation of the fluid drag coefficients in (1).

The model of the 8-arm system was developed in the SIMUUN computational environment [15], which is based on the SimMechanics toolbox of Simulink. The parameters describing the mechanical structure (masses, dimensions, etc.) were defined such that they match those of the robotic prototype of Section IV. The internal shape of the arms in the computational model was accomplished by explicitly prescribing the angular trajectories of the rotary joints φ_i^j (where j denotes the arm designation, see Fig. 2), while the fluid-arm interactions were described using the fluid drag model detailed in the previous paragraph, Eq. (1). For the latter, the drag coefficients developed on each arm segment by the flow were accurately computed by CFD methods [4], [5], while the fluid force coefficients for the main body segment were approximated with known theoretical values of drag, for flow over a circular disk of similar diameter.

The above computational framework was used, in this study, to simulate the 8-arm mechanism performing turning. Both the current investigation, which examines turning maneuvers, and the previous, in [3], which concerned straight-line multi-arm swimming by sculling and/or undulations, are extensions of the simpler, two-arm robot swimmer proposed in [5].

III. COMPUTATIONAL STUDIES

In general, any asymmetry in the relative motion between the arms will tend to cause deviations of the robot from a straight path. Turning may, therefore, be instigated by a number of different strategies, which involve specifying different values for one (or more) parameters of the arms' motions.

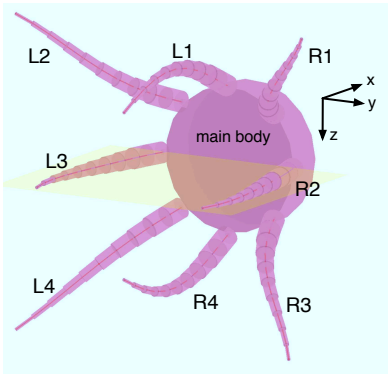

(a)

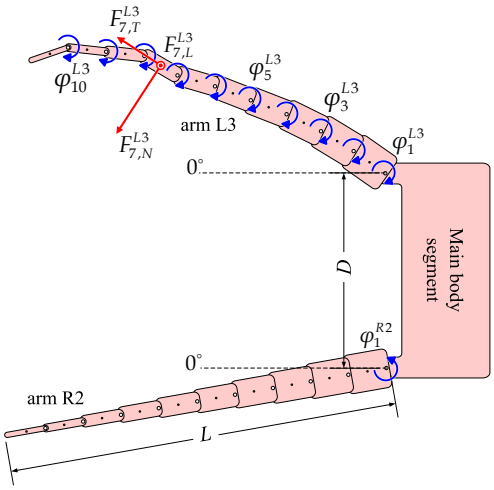

(b)

Fig. 2: (a) Configuration of the 8-arm swimming mechanism. (b) Planar view of a pair of diametrically opposite arms.

A. Arm sculling motion profile

The basic motion profile adopted to simulate the movement of individual arms is based on a two-stroke pattern, of different velocity ratio β between a relatively slow opening part (recovery stroke) and a considerably fast closing part (power stroke) of the arms. This mode of motion is termed *sculling* (Fig. 3) and can be considered as a first approximation of the octopus arm-swimming motion [3]. The main parameters describing the sculling profile are the arm rotation angle $\varphi(t)$, the sculling amplitude A, the sculling offset ψ, the recovery (base) velocity ω and the velocity ratio β.

With the sculling mode, each individual arm is connected to the main body with a periodic, two-stroke angular function $\varphi_1(t)$, while it moves as a straight unit, by applying $\varphi_i = 0$ for the inter-linked segments ($i = 2..n$). The angle $\varphi_1(t)$ was implemented by using the following acceleration profile (as shown in Fig. 3), integrated twice, with $\dot{\varphi}_1(0) = 0$ and

Preprint submitted to 21st Mediterranean Conference on Control and Automation.
Received February 22, 2013.

$\varphi_1(0) = \psi - A$, where $2A$ is the total angular span:

$$\ddot{\varphi}_1(t) = \begin{cases} \alpha_0 \sin\left(\dfrac{\pi t}{0.2T_r}\right) & 0 \le t < 0.2T_r \\ 0 & 0.2T_r \le t < 0.8T_r \\ -\alpha_0 \sin\left(\dfrac{\pi(t-0.8T_r)}{0.2T_r}\right) & 0.8T_r \le t < T_r \\ \beta\alpha_0 \sin\left(\dfrac{\pi(t-T_r)}{0.2T_p}\right) & 0 \le t - T_r < 0.2T_p \\ 0 & 0.2T_p \le t - T_r < 0.8T_p \\ -\alpha_0 \sin\left(\dfrac{\pi(t-T_r-0.8T_p)}{0.2T_p}\right) & 0.8T_p \le t - T_r < T_p, \end{cases}$$

It is noted that positive values of φ_1 correspond to the arm being extended outwards, as indicated in Fig. 2b. The above expression gives a smooth motion profile for the angular velocity, both for the power and recovery strokes, that enables their successful application through the actuators of the robotic prototype (see Section IV). According to this sculling profile, the angular velocity during the power and the recovery stroke is maintained at its maximum absolute values of $\beta\omega$ and ω, respectively, for 60% of the stroke's duration. In addition, the maximum absolute acceleration for the power and recovery strokes is $\beta\alpha_0$ and α_0, respectively, where $\beta > 1$ and $a_0 = 2\pi\omega^2/A$. The overall time duration of the two strokes is, respectively: $T_p = 2.5A/(\beta\omega)$ and $T_r = \beta T_p$, whereas the total time period of the motion is: $T_s = T_p + T_r = (\beta + 1)T_p$.

B. Turning gaits

Turning can, hence, be generated by a variety of asymmetric motions of the robot's arms, through sculling and/or undulatory movements, that result in a range of "turning gaits". Indeed, multiple such gaits could be implemented by appropriate arm coordination in any three-dimensional direction. An example is shown in Fig. 4, where the system performs a turn on the xy plane by specifying asymmetric combinations of sculling and undulations for oppositely-positioned lateral groups of arms, e.g., {L2, L3, L4} and {R1, R2, R3}, while keeping the other motion parameters fixed. Similar movements could be performed in any other plane or in the 3D space by defining different arm combinations. It is also possible to devise several variations of these gaits, e.g. by altering the phase between the arms.

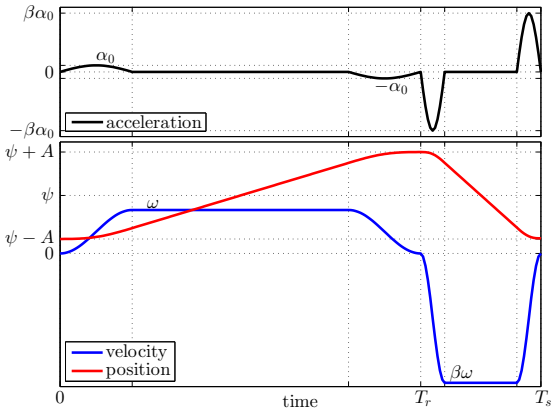

Fig. 3: Sculling motion profile.

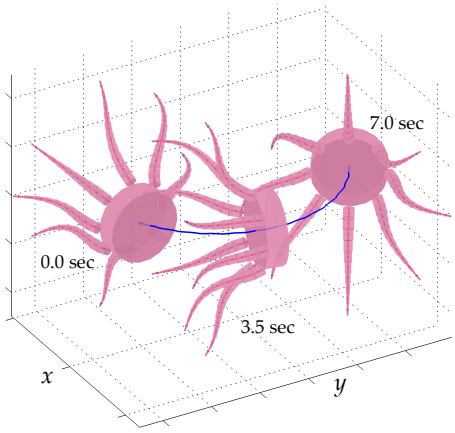

Fig. 4: Simulation result for turning movement with a combination of sculling and arm undulations.

In order to systematically study turning on the 8-arm mechanism presented, and facilitate its implementation on the robotic prototype (see Section IV), here, we focus our investigation on planar turning gaits using sculling-only movements of rigid arms (i.e., where $\varphi_i = 0$, $i = 2..10$, for all eight arms in the model of Fig. 2b). Three such turning gaits are presented here, as follows:

GR1 gait: The first turning gait is generated by the synchronized sculling movement of three adjacent arms on the same side of the device, e.g., {L2, L3, L4}, while the remaining five arms are extended outwards, at the maximum angular position, i.e. at $(\psi + A)$. The trajectory obtained with this gait, as well as the temporal variation of the arm's angle and of the turning rate of the main body is presented in Fig. 5a.

GR2 gait: The second turning gait is produced by the synchronized sculling movement of three opposite pairs of lateral arms, namely {R1, L4}, {R2, L3}, and {R3, L2}, each pair moving in each one plane, while the remaining two arms, {L1} and {R4}, are extended outwards at the maximum angular position $(\psi + A)$. An indicative trajectory of this gait is shown in Fig. 6.

GR3 gait: This gait is achieved by the synchronized sculling movement of three opposite pairs of lateral arms, {R1, L4}, {R2, L3}, and {R3, L2}, of which, however, three adjacent arms at one of the sides, {R1, R2, R3}, are performing the sculling motion at half the amplitude of the ones at the other side (at the same T_s). Arms {L1} and {R4} are extended outwards at the maximum angular position $(\psi + A)$. Indicative results are shown in Fig. 7.

The computational framework presented in Section II, was employed to investigate the characteristics of turning by gaits $GR1$, $GR2$ and $GR3$, through a series of parametric studies. In all of the simulations shown here, the angular velocity of each arm during the recovery stroke was set at $\omega = 50°/\text{s}$, while the velocity ratio was selected as $\beta = 5$.

Indicative simulation results are provided in Figs. 5-7, where, for all three gaits, the sculling amplitude and sculling offset were specified as $A = 25°$ and $\psi = 30°$, respectively. The trajectory plots in these figures indicate that gaits $GR1$ and $GR2$ essentially implement in-place rotation (with, however, different characteristics), while $GR3$ appears to be more

Preprint submitted to 21st Mediterranean Conference on Control and Automation.
Received February 22, 2013.

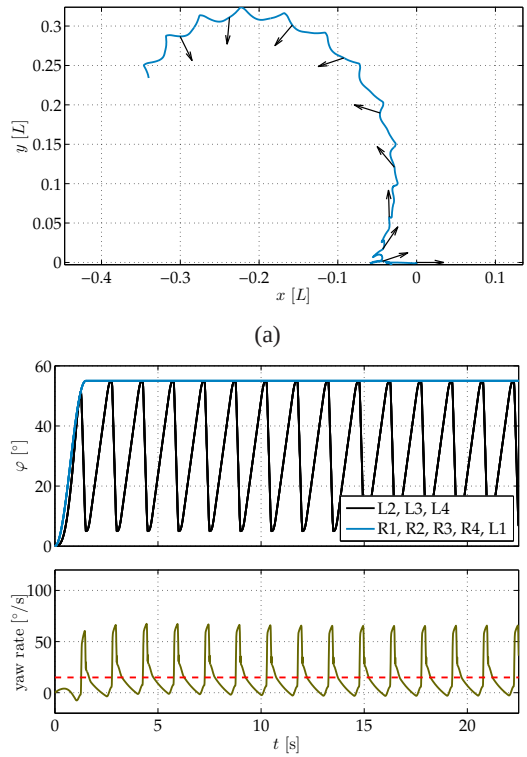

Fig. 5: Simulation results for gait $GR1$: (a) Trajectory of the center of mass of the main body, over a time period corresponding to 15 sculling periods. The axes are normalized with respect to the arm length L, while the arrows indicate the heading direction of the main body, at the start of each recovery stroke. (b) Temporal variation of the arms' angle (top), and of the turning rate of the main body (bottom). The dashed red line indicates the average yaw rate at steady-state ($A = 25°$, $\psi = 30°$, $\omega = 50°/\text{s}$, $\beta = 5$).

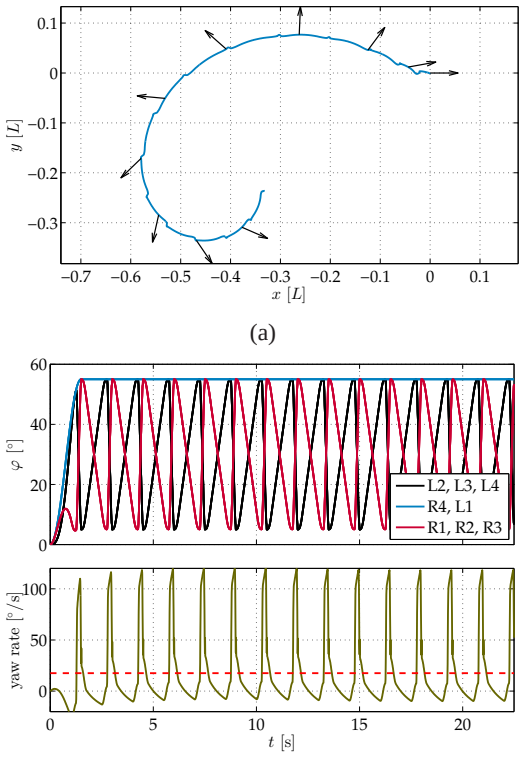

Fig. 6: Simulation results for gait $GR2$ (see caption of Fig. 5).

appropriate for combining heading direction changes with an overall translational motion (c.f. also Fig. 9). Furthermore, the plots with the temporal evolution of the yaw angular velocity indicate that the latter exhibits a higher average value, as well as larger variance during each sculling period, for $GR2$.

The stride angle, representing the average angle by which the heading direction changes during each sculling stroke, is shown in Fig. 8. The results indicate that, for all three of the investigated turning gaits, the attained stride angle is reduced as the sculling offset ψ is increased, and increases with the sculling amplitude A. Moreover, in line with the observations regarding Figs. 5-7, it can be seen that the highest stride angles are obtained with $GR2$, while $GR3$ is the least effective of the three gaits in incurring rapid changes in the heading direction of the system.

In addition, Fig. 9 shows the effect of the sculling offset angle ψ on the trajectory of the system, for the three investigated gaits. The results suggest that, for $GR1$ and $GR3$, the turning radius increases with ψ, while there is little dependence between the two in the case of $GR2$.

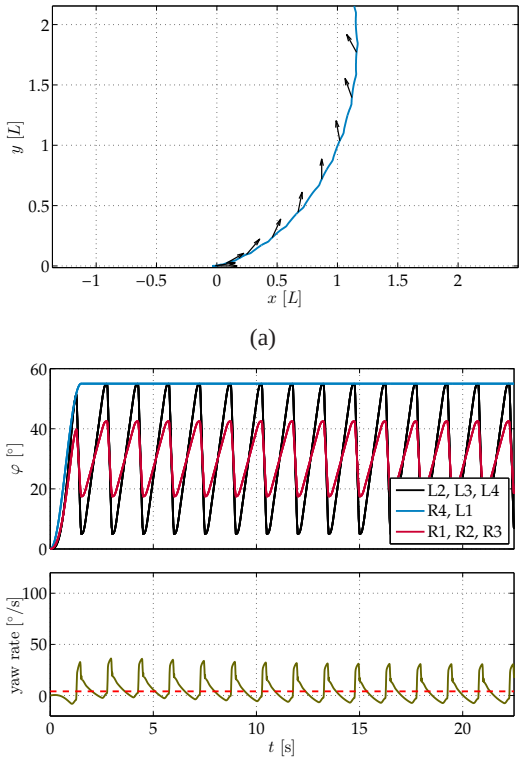

Fig. 7: Simulation results for gait $GR3$ (see caption of Fig. 5).

Preprint submitted to 21st Mediterranean Conference on Control and Automation.
Received February 22, 2013.

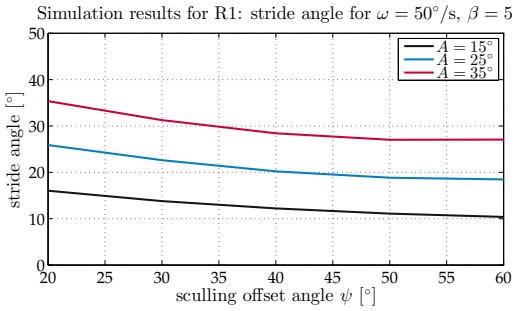

(a) Gait $GR1$

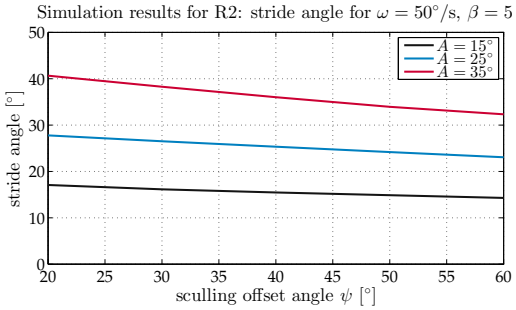

(b) Gait $GR2$

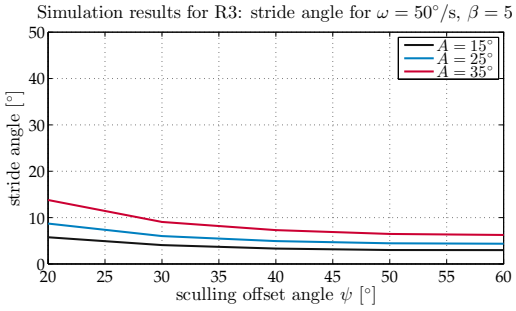

(c) Gait $GR3$

Fig. 8: Simulation results: Attained stride angle as a function of the sculling offset ψ and the sculling amplitude A, for the three proposed turning gaits.

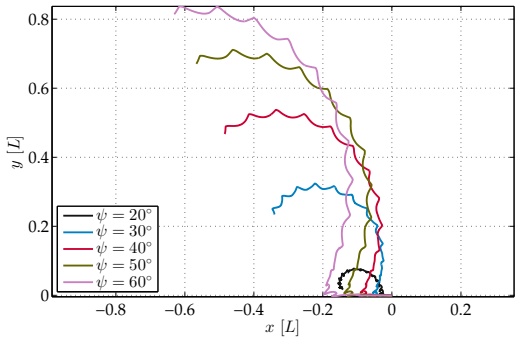

(a) Gait $GR1$

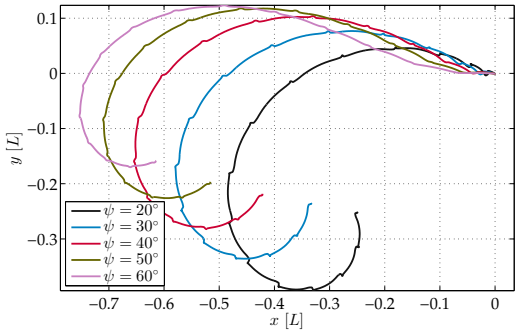

(b) Gait $GR2$

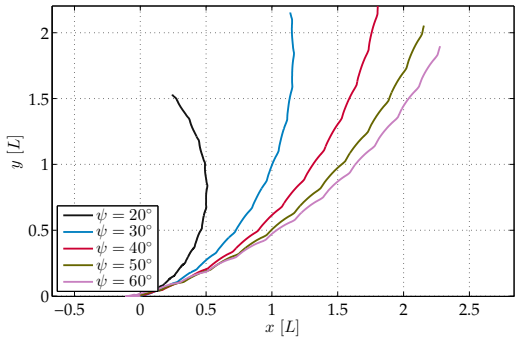

(c) Gait $GR3$

Fig. 9: Simulation results: Trajectory of the center of mass of the main body, for different sculling offset angles (obtained with $A = 25°$), for the three proposed turning gaits. The axes are normalized with respect to the arm length L.

IV. ROBOTIC EXPERIMENTS

A. Setup

An 8-arm robotic prototype was developed in order to experimentally explore the multi-arm maneuverability of such systems (Fig. 10). The current prototype is an extension of the one developed in [3], for straight-line locomotion, in that it is energetically autonomous (powered by a battery), and fully untethered (within the limits of the experimental water tank: 200 cm in length, 70 cm in width, and 60 cm in height).

The prototype was manufactured in a 3D printer (Elite, Dimension, USA) using ABSplus material. Each of the eight rigid arms, which were also made of ABSplus, included 38 octopus-like 'suckers'of cylindrical shape, positioned in a staggered arrangement, according to [4]; the arm's base- and tip-diameters were 20 mm and 2 mm, respectively, and its length was 200 mm. The arms were controlled by individual waterproof micro-servomotors (HS-5086WP, Hitech, USA), capable of rotating over a span of approximately 110°. An octagonal platform, of diameter 15.5 cm, was built by the same ABSplus material to allow mounting of the servomotors (Fig. 10a-III). The platform was especially designed such that pairs of arms in diametrically-opposite positions can move in the same plane, as in the computational model. An *Arduino pro mega* microcontroller platform is employed for independently controlling the 8 servomotors of the prototype, in order to implement the various turning gaits. Wireless communication of this microcontroller with a host PC is achieved through a dedicated RF link. All electronics and connection cables are housed inside a waterproof case,

Preprint submitted to 21st Mediterranean Conference on Control and Automation.
Received February 22, 2013.

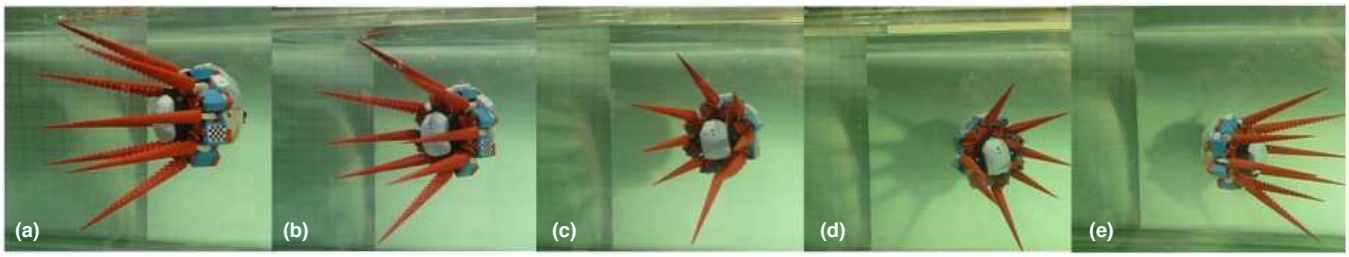

Fig. 11: Robotic prototype performing turning gait $GR3$ with $A = 15°$, $\psi = 20°$, $\omega = 60°/\,\mathrm{s}$ and $\beta = 5$, at intervals of 6 time periods (T_s): $t =$ (a) $6T_s$, (b) $12T_s$, (c) $18T_s$, (d) $24T_s$, (e) $30T_s$.

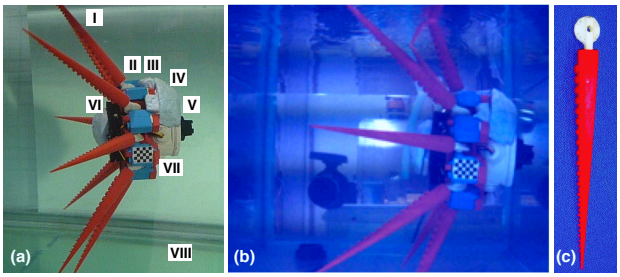

Fig. 10: (a) 8-arm robotic prototype captured with an external camera: (I) arms, (II) servomotors, (III) platform, (IV) buoyancy attachments, (V) electronics housing box, (VI) battery housing case, (VII) checkerboard marker, and (VIII) water tank space. (b) Snapshot obtained by the high-definition underwater camera. (c) One rigid arm.

mounted at the front side of the prototype (Fig. 10a-V). A Li-Po battery, placed inside a rear-mounted waterproof housing (Fig. 10a-VI), allows for about 1 hour of continuous operation of the robot. The overall weight of the submerged prototype is 1.1 kg. The operational depth of the swimmer was passively regulated by buoyancy attachments made of foam (Fig. 10a-IV).

Information about the position and orientation of the robotic prototype during each gait was obtained by a high-definition underwater camera, via computer vision methods. By mounting a 2D checkerboard marker of known size on the robotic platform, the intrinsic calibration of the camera was performed, with a strong estimation of the camera parameters. The 3D trajectories of the robotic platform were estimated through a process that first calculated the homography between two images, one of the camera's plane and one of the marker's plane, up to a scale factor, and, then, used nonlinear minimization [16] to estimate the maximum likelihood of the orientation and position of the marker, based on the calculated homography, as initial guess.

B. Experimental results

Experiments with the robotic prototype demonstrated the generation of propulsion via sculling arm movements, and confirmed that appropriately selected asymmetries in these sculling movements (as per the proposed turning gaits) are an effective means of obtaining turning maneuvers.

More specifically, snapshots from an indicative trajectory of the system, for gait $GR3$ ($A = 15°$, $\psi = 20°$, $\omega = 60°/\,\mathrm{s}$ and $\beta = 5$), are shown in Fig. 11. Initially, the robot is oriented towards the right and then, an almost $180°$ turn is shown to be achieved over a duration of 24 sculling periods (corresponding to 18s)[1].

A composite plot, showing indicative trajectories for the three turning gaits considered, obtained with the same set of parameters ($A = 25°$, $\psi = 40°$, $\omega = 50°/\,\mathrm{s}$ and $\beta = 5$), is provided in Fig. 12. These can be seen to be qualitatively consistent with the trajectories obtained in simulation (c.f. Figs. 5-7)

Qualitative agreement is also evident in the yaw angular velocity profile for $GR2$ (shown in Fig. 13) when compared with the simulation result of Fig. 6b. Analogous agreement also exists for other gaits and parameters.

Finally, estimates for the average stride angle attained by the robotic swimmer, as a function of the sculling amplitude and sculling offset, are provided, for all three turning gaits, in Fig. 14. Much as in the corresponding simulation results (c.f. Fig. 8), the stride angles for gaits $GR1$ and $GR2$ are similar and larger than the ones for gait $GR3$, and the stride angle appears to increase as the sculling amplitude increases.

The discrepancies observed when comparing the experimental results with those from the simulations may be due to various reasons, including inaccuracies in the specifications of the modeling parameters and limitations of the fluid drag model used, imperfect buoyancy compensation, as well as inherent limitations and performance variability of the servomotors used in the prototype.

It is worth noting, that the computational and experimental methodology employed here is analogous to the one used in [3] for the analysis of swimming in a straight line by sculling arm movements. The agreement between simulation and experimental results, in that case, was more evident (quantitatively, as well as qualitatively) than in the present study. This may indicate that shortcomings in our experimental setup (e.g., boundary effects due to the limited width of the water tank, and difficulties in the acquisition of the visual data due to the limited field of view of the underwater camera) have a more significant impact when studying turning maneuvers.

[1]Supplementary video can be downloaded from:
$http://dl.dropbox.com/u/40834244/MED13\_FORTH.mp4$

Preprint submitted to 21st Mediterranean Conference on Control and Automation.
Received February 22, 2013.

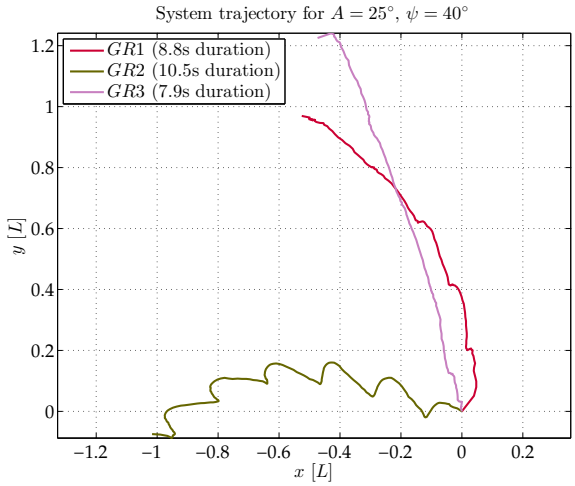

Fig. 12: Experimental results: Trajectories obtained for the three turning gait for a common set of sculling parameters.

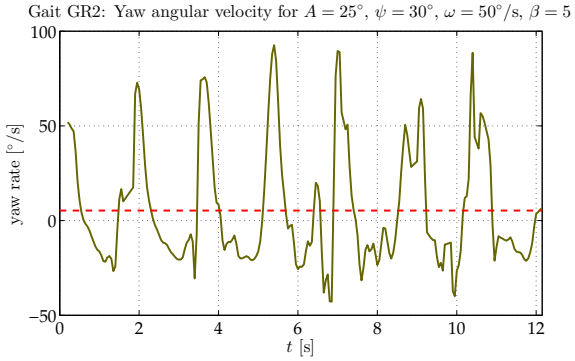

Fig. 13: Experimental results: Temporal variation of the yaw velocity, estimated from the visual tracking system, for gait $GR2$. The dashed red line indicates the average yaw rate at steady-state.

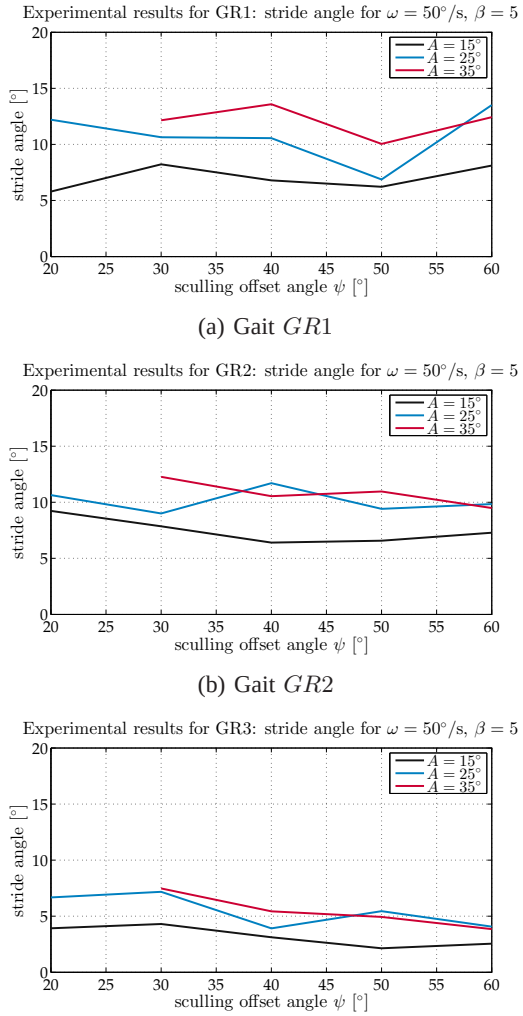

Fig. 14: Experimental results: Attained stride angle as a function of the sculling offset ψ and the sculling amplitude A, for the three proposed turning gaits.

V. CONCLUSIONS

In this paper, we focus on the generation of a novel turning behavior for an octopus-inspired 8-arm robotic swimmer, utilizing exclusively arm movements, rather than the more usual jetting propulsion mechanism. The system is tested, both computationally and experimentally, in free swimming conditions under various turning gaits, based on sculling arm movements. The tests aimed at assessing the effect of the various kinematic parameters of the developed gaits. The experimental results are in good qualitative agreement with those from the simulations.

These studies are expected to provide the foundation for developing complete reactive behaviors of the swimmer, which will appropriately combine straight-line and turning movements, and for devising corresponding closed-loop control strategies based on sensory information.

Further future studies will take into account detailed kinematic data extracted from recordings of octopus arm swimming. In addition, movements with compliant arms, an octopus-like web, and actively-controlled, multi-joint arms for the implementation of undulatory-based gaits, will be considered.

VI. ACKNOWLEDGMENTS

The authors would like to thank B. Hochner, M. Kuba, T. Flash and F. Grasso for insightful discussions. Also, A. Hatzidaki, Th. Evdemon, S. Stefanou, N. Pateromichelakis, X. Zabulis, and J.A. Ekaterinaris for their assistance with these studies.

REFERENCES

[1] E. G. Drucker and G. V. Lauder, "Wake dynamics and fluid forces of turning maneuvers in sunfish," *J. Exp. Biol.*, vol. 204, pp. 431–442, 2001.

[2] A. Kazakidi, M. Kuba, A. Botvinnik, M. Sfakiotakis, T. Gutnick, S. Hanassy, G. Levy, J. A. Ekaterinaris, T. Flash, B. Hochner, and D. P. Tsakiris, "Swimming patterns of the octopus vulgaris," in *22nd Annual Meeting NCM Society*, Venice, Italy, April 23-29, 2012.

[3] M. Sfakiotakis, A. Kazakidi, N. Pateromichelakis, and D. P. Tsakiris, "Octopus-inspired eight-arm robotic swimming by sculling movements," in *IEEE Int. Conf. Rob. Autom. (ICRA'13)*, Karlsruhe, Germany, May 6-10, 2013 (accepted for publication).

Preprint submitted to 21st Mediterranean Conference on Control and Automation.
Received February 22, 2013.

[4] A. Kazakidi, V. Vavourakis, N. Pateromichelakis, J. Ekaterinaris, and D. P. Tsakiris, "Hydrodynamic analysis of octopus-like robotic arms," in *IEEE Int. Conf. Rob. Autom. (ICRA'12)*, St. Paul, Minnesota, USA, May 14-18, 2012, pp. 5295–5300.
[5] M. Sfakiotakis, A. Kazakidi, N. Pateromichelakis, J. Ekaterinaris, and D. P. Tsakiris, "Robotic underwater propulsion inspired by the octopus multi-arm swimming," in *IEEE Int. Conf. Rob. Autom. (ICRA'12)*, St. Paul, Minnesota, USA, May 14-18, 2012, pp. 3833–3839.
[6] Y. Gutfreund, T. Flash, Y. Yarom, G. Fiorito, I. Segev, and B. Hochner, "Organization of octopus arm movements: A model system for studying the control of flexible arms," *J. Neurosc.*, vol. 16, 1996.
[7] I. Walker, D. Dawson, T. Flash, F. Grasso, R. Hanlon, B. Hochner, W. Kier, C. Pagano, C. Rahn, and Q. Zhang, "Continuum robot arms inspired by cephalopods," in *Proc. SPIE Conf. on Unmanned Ground Vehicle Technology IV*, vol. 5804, no. 37, 2005, pp. 303–314.
[8] C. Laschi, B. Mazzolai, V. Mattoli, M. Cianchetti, and P. Dario, "Design of a biomimetic robotic octopus arm," *Bioinspir. Biomim.*, vol. 4, no. 1, pp. 015 006–1–8, 2009.
[9] R. Kang, A. Kazakidi, E. Guglielmino, D. Branson, D. Tsakiris, J. Ekaterinaris, and D. Caldwell, "Dynamic model of a hyper-redundant, octopus-like manipulator for underwater applications," in *Proc. IEEE/RSJ Int. Conf. on Int. Rob. Syst. (IROS'11)*, San Francisco, CA, September 25-30, 2011, pp. 4054–4059.
[10] J. Mather, "How do octopuses use their arms?" *J. Comparative Psychology*, vol. 112, no. 3, pp. 306–316, 1998.
[11] G. Taylor, "Analysis of the swimming of long and narrow animals," *Proc. Roy. Soc. A*, vol. 214, pp. 158–183, 1952.
[12] Ö. Ekeberg, "A combined neuronal and mechanical model of fish swimming," *Biol. Cybern.*, vol. 69, no. 5-6, pp. 363–374, 1993.
[13] A. Ijspeert, "A connectionist central pattern generator for the aquatic and terrestrial gaits of a simulated salamander," *Biol. Cybern.*, vol. 85, no. 5, pp. 331–348, 2001.
[14] K. A. McIsaac and J. P. Ostrowski, "Experimental verification of open-loop control for an underwater eel-like robot," *Int. J. Rob. Res.*, vol. 21, pp. 849–860, 2002.
[15] M. Sfakiotakis and D. Tsakiris, "SIMUUN: A simulation environment for undulatory locomotion," *Int. J. Model. Simul.*, vol. 26, no. 4, pp. 4430–4464, 2006.
[16] Z. Zhang, "Flexible camera calibration by viewing a plane from unknown orientations," *Proc. IEEE Int. Conf. Comp. Vision (ICCV'99)*, pp. 666–673, 1999.

Preprint submitted to 21st Mediterranean Conference on Control and Automation.
Received February 22, 2013.